



University of Pennsylvania  
ScholarlyCommons

Departmental Papers (Chemistry)

Department of Chemistry

6-1-2007

# Fluorescence Correlation Spectroscopic Study of Serpin Depolymerization by Computationally Designed Peptides

Pramit Chowdhury

Wei Wang


Stacey Lavender  
*University of Pennsylvania*

Michelle R Bunagan  
*University of Pennsylvania*

Jason W. Klemke

*See next page for additional authors*

Follow this and additional works at: [http://repository.upenn.edu/chemistry\\_papers](http://repository.upenn.edu/chemistry_papers)

 Part of the [Biochemistry Commons](#), and the [Organic Chemistry Commons](#)

## Recommended Citation

Chowdhury, P., Wang, W., Lavender, S., Bunagan, M., Klemke, J. W., Tang, J., Saven, J. G., Cooperman, B. S., & Gai, F. (2007). Fluorescence Correlation Spectroscopic Study of Serpin Depolymerization by Computationally Designed Peptides. *Journal of Molecular Biology*, 369 (2), 462-473. <http://dx.doi.org/10.1016/j.jmb.2007.03.042>

This paper is posted at ScholarlyCommons. [http://repository.upenn.edu/chemistry\\_papers/3](http://repository.upenn.edu/chemistry_papers/3)  
For more information, please contact [repository@pobox.upenn.edu](mailto:repository@pobox.upenn.edu).

---

# Fluorescence Correlation Spectroscopic Study of Serpin Depolymerization by Computationally Designed Peptides

## Abstract

Members of the serine proteinase inhibitor (serpin) family play important roles in the inflammatory and coagulation cascades. Interaction of a serpin with its target proteinase induces a large conformational change, resulting in insertion of its reactive center loop (RCL) into the main body of the protein as a new strand within beta-sheet A. Intermolecular insertion of the RCL of one serpin molecule into the beta-sheet A of another leads to polymerization, a widespread phenomenon associated with a general class of diseases known as serpinopathies. Small peptides are known to modulate the polymerization process by binding within beta-sheet A. Here, we use fluorescence correlation spectroscopy (FCS) to probe the mechanism of peptide modulation of alpha(1)-antitrypsin (alpha(1)-AT) polymerization and depolymerization, and employ a statistical computationally-assisted design strategy (SCADS) to identify new tetrapeptides that modulate polymerization. Our results demonstrate that peptide-induced depolymerization takes place via a heterogeneous, multi-step process that begins with internal fragmentation of the polymer chain. One of the designed tetrapeptides is the most potent antitrypsin depolymerizer yet found.

## Keywords

Amino Acid Sequence, Models, Molecular, Peptides, Protein Structure, Quaternary, Serpins, Spectrometry, Fluorescence, alpha 1-Antitrypsin

## Disciplines

Biochemistry | Organic Chemistry

## Author(s)

Pramit Chowdhury, Wei Wang, Stacey Lavender, Michelle R Bunagan, Jason W. Klemke, Jia Tang, Jeffery G. Saven, Barry S. Cooperman, and Feng Gai

# Fluorescence Correlation Spectroscopic Study of Serpin Depolymerization by Computationally Designed Peptides

Pramit Chowdhury, Wei Wang, Stacey Lavender, Michelle R. Bunagan, Jason W. Klemke, Jia Tang, Jeffrey G. Saven\*, Barry S. Cooperman\*, and Feng Gai\*  
*Department of Chemistry, University of Pennsylvania, Philadelphia, PA 19104*

## SUMMARY

Members of the serine proteinase inhibitor (serpin) family play important roles in the inflammatory and coagulation cascades. Interaction of a serpin with its target proteinase induces a large conformational change, resulting in insertion of its reactive center loop (RCL) into the main body of the protein as a new strand within  $\beta$ -sheet A. Intermolecular insertion of the RCL of one serpin molecule into the  $\beta$ -sheet A of another leads to polymerization, a widespread phenomenon associated with a general class of diseases known as serpinopathies. Small peptides are known to modulate the polymerization process by binding within  $\beta$ -sheet A. Here we use fluorescence correlation spectroscopy (FCS) to probe the mechanism of peptide modulation of  $\alpha_1$ -antitrypsin ( $\alpha_1$ -AT) polymerization and depolymerization, and employ a statistical computationally-assisted design strategy (SCADS) to identify new tetrapeptides that modulate polymerization. Our results demonstrate that peptide-induced depolymerization takes place via a heterogeneous, multi-step process which begins with internal fragmentation of the polymer chain. One of the designed tetrapeptides is the most potent antitrypsin depolymerizer yet found.

## Keywords

serpin polymerization;  $\alpha_1$ -antitrypsin; computer design; fluorescence correlation spectroscopy (FCS); serpin depolymerization

## INTRODUCTION

Serine proteinase inhibitors (serpins) are a superfamily of proteins that control a wide variety of biological events, such as inflammation, coagulation and fibrinolysis.<sup>1-4</sup> Serpin structure is characterized by the presence of a central  $\beta$ -sheet A (the largest of the three  $\beta$ -sheets) flanked by two shorter  $\beta$ -sheets B and C, and a mobile, inhibitory 14-residue reactive center loop (RCL) (see Figure 1).<sup>5-8</sup> The RCL directly interacts with the protease and can either remain fully exposed or upon proteolysis become partially or fully inserted into the five stranded  $\beta$ -sheet A.<sup>8-13</sup> More specifically, binding of a serpin to its target proteinase not only results in the cleavage of the RCL but also initiates a significant conformational change that ultimately results in residues P1 – P14 of the cleaved RCL incorporating into  $\beta$ -sheet A as  $\beta$ -strand s4A.<sup>5,7,8,14</sup> This process is commonly referred to as the S (stressed) to R (relaxed) transition during which the protease is translocated  $\sim 70$  Å from the proximal to the distal end of the serpin molecule. In addition, some serpins undergo spontaneous intramolecular insertion of the intact

\*To whom correspondence should be addressed: saven@sas.upenn.edu, cooprman@pobox.upenn.edu, gai@sas.upenn.edu

**Publisher's Disclaimer:** This is a PDF file of an unedited manuscript that has been accepted for publication. As a service to our customers we are providing this early version of the manuscript. The manuscript will undergo copyediting, typesetting, and review of the resulting proof before it is published in its final citable form. Please note that during the production process errors may be discovered which could affect the content, and all legal disclaimers that apply to the journal pertain.

RCL into the A  $\beta$ -sheet, leading to formation of a latent form that has a more stable fold than the active form.<sup>12-15</sup>

While an exposed RCL is necessary for serpin function, its proclivity to undergo  $\beta$ -sheet insertion makes serpin molecules vulnerable to polymerization. In the latter process, the RCL of one molecule inserts into the  $\beta$ -sheet of another, forming loop-sheet linkages<sup>16-21</sup> that appear on electron micrographs as flexible beads-on-a-string.<sup>7,19</sup> (See Figure 1.) Polymer formation sequesters a serpin in an inactive form and is associated with diseases such as thrombosis, angiodema and dementia.<sup>19</sup>  $\alpha_1$ -Antitrypsin ( $\alpha_1$ -AT) protects the lung tissues against the proteolytic action of the enzyme neutrophil elastase and its deficiency is the most extensively studied of the serpin related diseases, referred to collectively as 'serpinopathies'.<sup>19</sup> While over 70 naturally occurring  $\alpha_1$ -AT variants have been identified and characterized, the S (Glu<sup>264</sup>→Val) and Z (Glu<sup>342</sup>→Lys) variants are the most clinically relevant and arise as a result of point mutations in the  $\alpha_1$ -AT gene.<sup>19</sup> These mutations lead to formation of  $\alpha_1$ -AT polymers under physiological conditions that are retained in the endoplasmic reticulum of the liver, predisposing the homozygote to juvenile hepatitis, cirrhosis and hepatocellular carcinoma.<sup>22-26</sup>

Ensemble measurements of fluorescence and CD changes, coupled with PAGE analysis, have led to formulation of a two-step mechanism of  $\alpha_1$ -AT polymerization in which a relatively fast intramolecular conformational change within monomeric  $\alpha_1$ -AT is followed by a polymerization step involving intermolecular loop-sheet insertion.<sup>27-29</sup> In addition, the overall rate of polymerization has been shown to vary with concentration, temperature and pH.<sup>28,30,31</sup> More recently, using single-molecule fluorescence correlation spectroscopy (FCS) we have shown that  $\alpha_1$ -AT polymerization is a heterogeneous process that proceeds via a nucleation and growth model, whereby longer polymers form via the condensation of two shorter polymers, and in which the nature of the "nucleus" is a variable dependent on experimental conditions.<sup>31</sup> Despite this variability in the self-association process,  $\alpha_1$ -AT polymers show a clear preference for species having 8 to 16 monomer units, consistent with the results of electron microscopic analysis.<sup>7</sup>

Peptides corresponding to sequences within residues P<sub>14</sub>-P<sub>1</sub> of the RCL have been shown to anneal to the  $\beta$ -sheet A of a native serpin by a mechanism analogous to the loop-sheet insertion, thereby preventing further polymerization<sup>5,31-34</sup>. Recently, Zhou *et al.* have identified small peptides unrelated to the serpin RCL sequence that not only block the polymerization of  $\alpha_1$ -AT and antithrombin, but also depolymerize antithrombin polymers.<sup>35</sup> Although this study did not provide a detailed description of the mechanism of the depolymerization process, it did include structural information showing that one such peptide, WMDF, occupies the P<sub>7</sub>-P<sub>4</sub> vacancy in s4A site of antithrombin such that the P<sub>6</sub> and P<sub>4</sub> sidechains (M and F) are bound in well-defined hydrophobic pockets.<sup>35</sup> Depolymerization results with other tetrapeptides reinforces the notion that effective disassembly of serpin polymers depends on binding hydrophobic residues into these pockets.

In this paper we use the results of Zhou *et al.* as a starting point both to probe the mechanism of small peptide-induced serpin depolymerization and to systematically design and identify short peptide sequences (tetrapeptides) that are effective in breaking up serpin polymers. Peptides likely to bind in the middle strand of the A  $\beta$ -sheet have been designed based on a statistical, computationally-assisted design strategy (SCADS).<sup>35-38</sup> SCADS considers the protein structure atomistically using a molecular force field and has been applied successfully to suggest solutions to several recent protein design problems.<sup>38-44</sup>

Depolymerization of a linear polymer can proceed either via sequential deletion of monomer units from the ends of the polymers or via fragmentation into shorter polymeric strands due to

cleavage between protein monomers within the polymer interior (see Figure 2). We distinguish between these possibilities by using fluorescence correlation spectroscopy (FCS) that measures the temporal intensity fluctuations caused by the diffusion of single fluorescent molecules into and out of a detection volume.<sup>45-57</sup> Such measurements allow the monitoring of the length distribution of species formed during polymerization and depolymerization, according to their respective diffusion times. Our results show that depolymerization proceeds via a heterogeneous, multi-step process which begins with internal fragmentation of the polymer chain, although later in the process both sequential deletion and fragmentation become important.

## RESULTS

### FCS measurement

As described previously,<sup>30</sup> the autocorrelation function,  $G(\tau)$ , obtained in a FCS experiment provides information about the residence time of a fluorescent molecule in the laser excitation volume element.<sup>49</sup> For a given confocal microscopy setup, the residence time,  $\tau_D$ , provides a direct measure of the molecule's diffusion constant and hydrodynamic radius (see Materials and Methods). Therefore, FCS is capable of measuring the size of a particle or molecular species diffusing through the confocal volume and can be used to examine the size distribution of the polymeric species at a specific reaction time during serpin polymerization or depolymerization. In addition, from the amplitude of the autocorrelation function at zero lag time ( $\tau=0$ ), i.e.,  $G(0)$ , one can also confirm the number of molecules within the volume element, and thus the sample concentration.<sup>45-49</sup> Because  $G(0)$  varies inversely with the number of molecules in the confocal volume, it increases during serpin polymerization, as shorter precursors are converted into longer polymers, and decreases during serpin depolymerization as longer polymers dissociate into shorter oligomers (see Figure 3).

### WMDF inhibition of $\alpha_1$ -AT polymerization

Earlier<sup>30</sup> we showed that, at least up to 55 °C, raising the temperature increases both the rate of formation and the average length of  $\alpha_1$ -AT polymers. The results presented in Figure 4 show that the added WMDF inhibits  $\alpha_1$ -AT polymerization at 39 °C, but does not block the formation of  $\alpha_1$ -AT polymers at 52 °C. Furthermore, preincubation of  $\alpha_1$ -AT with WMDF for 24 hours at 39 °C followed by increase of sample temperature to 52 °C led to the formation of longer polymeric species (data not shown). As WMDF inhibition of polymerization presumably involves competition for a common binding site in  $\alpha_1$ -AT, these results thus suggest that the polymeric forms of  $\alpha_1$ -AT are more stable than the WMDF- $\alpha_1$ -AT complex at 52 °C. A similar finding has also been reported by Parfrey *et al.* for a hexapeptide-Z-AT complex,<sup>58</sup> and is further supported by similar results with one of the designed peptides, VIKF (data not shown), as referred to below. Consequently, depolymerization studies with WMDF and other peptides were carried out at 39 °C.

### WMDF induction of the depolymerization of $\alpha_1$ -AT polymers

As shown in Figure 3, autocorrelation traces taken at different times of incubation of  $\alpha_1$ -AT polymers with WMDF clearly indicate a time-dependent depolymerization process, characterized by decreases in both  $G(0)$  and  $\tau_D$ . While either parameter is a reliable monitor of the polymerization/depolymerization process,<sup>30</sup> below we will use only  $\tau_D$  to characterize the size of the intermediate polymeric  $\alpha_1$ -AT species formed during the course of depolymerization.

A more detailed view of the depolymerization process induced by WMDF was obtained by determining the distributions of different diffusing species over a 24 day incubation period (see Figure 5). The distribution is initially dominated by the presence of species with  $\tau_D$  values in

the range of 27 – 35 ms (Day 1), corresponding to polymers consisting of 13 – 18  $\alpha_1$ -AT monomer units.<sup>30</sup> The initial distribution of the diffusion times is little changed during the first few days of the depolymerization reaction, corresponding to a lag phase. With increasing incubation time, especially from the 7<sup>th</sup> day onwards, faster diffusing species (e.g.,  $\tau_D = 12 - 15$  ms) appear, consistent with depolymerization. From this point, the shift in the center of the distribution to smaller  $\tau_D$  values becomes more apparent, concomitant with the disappearance of species with longer diffusion times. Depolymerization is nearly complete by the 24<sup>th</sup> day, with a  $\tau_D$  distribution similar to that obtained on a freshly prepared monomeric  $\alpha_1$ -AT sample, which contains small amounts of dimer and trimer.<sup>30</sup>

### SCADS Design

We have used SCADS to design additional peptides that could not only block  $\alpha_1$ -AT self-assembly but also potentially reverse  $\alpha_1$ -AT polymerization efficiently. This method yields the site-specific probabilities of the amino acids at variable positions in a particular structure (or structural template) and its details have been described elsewhere.<sup>36-38</sup> In the current study, the x-ray crystal structure of the antithrombin-WMDF complex (pdb code: 1JVQ)<sup>35</sup> was used as the structural template to re-design tetrapeptide sequences that are effective in blocking  $\alpha_1$ -AT polymerization. For these sequence calculations, the coordinates of the peptide backbone atoms were constrained to those of the WMDF peptide. Only four sites are allowed to mutate, those residing on the peptide (P7-P4). All the other residues, including those of antithrombin, were fixed in their wild type conformations as presented in the protein databank structure 1JVQ.<sup>35</sup> Because the peptide is buried within the antithrombin structure, no effective solvation energies were used in the calculations.<sup>37</sup> The wild type peptide WMDF has only one charged residue. Hence, it is of interest to relocate the position of the ionizable group to each of the four positions. The sequences were thus constrained to have one charged residue and three hydrophobic residues, resulting in four computationally identified blocking peptides, each having an ionizable amino acid (K, R, E, D) at one of the four sites. Two rounds of calculations were performed. In the first round, all 20 amino acids were allowed at all four positions (position P7-P4), and all four sites were varied simultaneously. This first round of calculation identified those sites having a strong preference for an ionizable amino acid (R, K, D or E). In the second round, each of the four sites was targeted for an ionizable amino acid. For a given targeted position of a charged amino acid: if the first round calculation indicated that R, K, D, or E was most probable at the targeted position, the identity was fixed to this most probable amino acid and the remaining sites were varied; otherwise, only charged amino acids (R, K, D and E) were allowed. In each case, at the remaining three positions, only hydrophobic amino acids were permitted (A, V, I, L, W, F, M and G). After this second round of calculation, the identities of all sites were determined as the most probable amino acids at each site. These calculations yielded four sequences, with ionizable amino acids at sites P7 through P4, respectively: DIIF, VEIF, VIKF, and VIID. Note the dissimilarity between these peptides and WMDF; even the designed peptide with an ionizable group targeted at the P5 position (D in WMDF) has an amino acid (K) of opposite charge.

### Depolymerization of $\alpha_1$ -AT polymers by designed peptides

Only two of the four SCADS-designed peptides, VIKF and VEIF, were sufficiently soluble in aqueous buffer to be useful in studies of  $\alpha_1$ -AT depolymerization. The depolymerization process induced by VIKF (see Figure 6) gave results similar to those obtained with WMDF, but proceeded with an overall rate that was noticeably faster (compare, for example, the distributions obtained after 7<sup>th</sup> day of incubation in Figures 5 and 6). Depolymerization was confirmed at the ensemble level by nondenaturing PAGE analysis (Figure 7). Such analysis shows a dominant monomer band for unheated TMR-labeled  $\alpha_1$ -AT, and confirms the shift to highly aggregated forms on prolonged heating at 45 °C, a large fraction of which are unable to enter into the gel. Incubation of the aggregated protein for 21 days in the presence of VIKF

at 39 °C results in conversion to monomers, which is even more complete than what is seen for the unheated sample.

The overall average diffusion times as a function of the incubation period are compared in Figure 8 for VIKF, VEIF, WMDF, and FLKK. The latter served as a negative control since it was selected on the basis of its inconsistency with the computationally determined site-specific probabilities. These results, showing VIKF and VEIF to effectively induce depolymerization whereas FLKK does not, indicate that SCADS provides a promising approach to the design of small peptides capable of inducing depolymerization. Reducing peptide concentration from 200  $\mu\text{M}$  to 25  $\mu\text{M}$  led to much slower rates of depolymerization (data not shown).

Depolymerization induced by WMDF, VIKF, and VEIF proceeds via what appears to be a four-phase process. An initial lag phase of 5 – 7 days over which  $\tau_D$  maintains an average value of 26 – 28 ms is followed by a decrease over several days to reach an apparent plateau characterized by an average  $\tau_D$  value of 15 – 18 ms. The duration of this plateau phase, which is clearly visible in the case of VEIF but also discernible with WMDF and VIKF, is variable (2 – 7 days), and is followed by another decrease toward a final value of  $\sim 2$  ms.

## DISCUSSION

Serpin polymerization resulting from aberrant  $\beta$ -sheet aggregation leads to a variety of diseases.<sup>1,2,13,19,22,23</sup> Several studies have focused on identifying peptides that may prevent<sup>5,31-33</sup>, or even reverse<sup>35</sup> this process. While these studies have shown promising results, the methods used are nevertheless empirical, qualitative and not structure-based. A more rational design approach that leverages the structural information available for serpins and serpin-peptide complexes should facilitate the discovery of sequences having potential therapeutic applications. Using FCS, we investigated the size distribution of polymeric species during  $\alpha_1$ -AT depolymerization in the presence of WMDF and several designed peptides. Not only do the results verify the effectiveness of the computationally designed sequences, but they also provide new insights into the understanding of the mechanism of serpin depolymerization, a process about which little had been known heretofore.

### Mechanism of depolymerization

The results presented above permit some initial conclusions and speculations regarding the mechanism of peptide-induced depolymerization of  $\alpha_1$ -AT polymers. Inspection of Figures 5 and 6 shows that formation of species with  $\tau_D$  values  $\leq 6$  ms (monomers to trimers) only takes place during the third and fourth phases of depolymerization (see Figure 8), so that the decrease in  $\tau_D$  values during the second phase must arise exclusively via internal fragmentation of the polymer chains. This is essentially the reverse of our previous observation that, during  $\alpha_1$ -AT polymerization, the final, condensation of shorter oligomers.<sup>30</sup> Consequently, the second phase of depolymerization can be viewed as the reversal of the final phase of the polymerization process, with the first phase (or lag period) plausibly attributed to peptide binding and conformational changes accompanying such binding.

While WMDF and VEIF display very similar first and second phases of depolymerization, the third phase is markedly longer for VEIF. A possible interpretation of this difference is that transition to the 4<sup>th</sup> phase may require peptide interaction with a binding site that is distinct from the one involved in phases 1 and 2. The time-dependent distributions shown in Figures 5 and 6 should allow formulation of a quantitative model for the depolymerization process, and efforts in this direction are underway.

## Insights from the designed sequences

The designed peptides can be used to explore the allowed amino acids at each position of the tetrapeptide. As suggested in a previous study,<sup>35</sup> the P4 and P6 positions prefer less polar amino acids, since these residues may insert into hydrophobic pockets in the region where they bind to the protein (see Figure 9). This might be the reason why VEIF has the least efficiency among the three peptides shown in Figure 8. Glutamic acid being a negatively charged residue at the P6 position may give rise to unfavorable desolvation upon its entry into a hydrophobic pocket, hence leading to lower affinity and consequently a delay in breaking up of  $\alpha_1$ -AT polymers. The increased efficiency of VIKF over WMDF may result from the facts that isoleucine (I) is more hydrophobic and less flexible than methionine (M), while valine (V) is both hydrophobic and sterically less demanding than tryptophan (W), thereby leading to better packing/binding of VIKF inside the cavity of  $\alpha_1$ -AT. The inability of FLKK to act as a blocking agent towards  $\alpha_1$ -AT polymerization highlights the intrinsic importance of having a hydrophobic residue at the P4 position for achieving a high binding affinity. This is consistent with the observation that peptides efficient in blocking and depolymerizing all have a phenylalanine (F) at the P4 position.<sup>35</sup>

Furthermore, while the current design sequences were generated based on the crystal structure of the antithrombin-WMDF complex,<sup>35</sup> they nevertheless prove to be effective even for disassembling  $\alpha_1$ -AT polymers. This is consistent with the similarity of the antithrombin and antitrypsin structures in the vicinity of the peptide binding site. Therefore, this study demonstrates the applicability of the SCADS method towards the design of peptide sequences for serpin depolymerization. When combined with more accurate structural templates that closer represent the target protein,  $\alpha_1$ -AT rather than antithrombin, the method may lead to the design of peptides with more efficient depolymerization properties. In addition, the method presented here can be extended to rationally design therapies involving both peptide and non-peptide mimetics that can be used to treat antitrypsin deficiencies. For example, it could be used to design peptides that primarily target the clinically relevant Z-form of antitrypsin rather than the normal (M) form.<sup>58</sup>

## CONCLUSION

In summary, we have used fluorescence correlation spectroscopy, a technique with single molecule sensitivity, to gain insights into the understanding of the serpin depolymerization mechanism by small peptides. The results show that depolymerization is indeed very heterogeneous in its evolution as observed from the multitude of species present. Depolymerization appears to proceed via a combination of internal fragmentation of polymers and sequential deletion of monomeric units (especially at the later stage of depolymerization). The SCADS method provides a systematic approach towards the rational design of short peptides that would not only block but also break-up preformed  $\alpha_1$ -AT polymers. One of the designed sequences shows improvement in the kinetic efficiency of serpin depolymerization compared to WMDF, indicating that such computer aided design approach is promising for future studies related to therapies relevant to serpinopathies.

## MATERIALS AND METHODS

### SCADS Design

In order to make a judicious choice for the selection of peptides that can efficiently block and reverse  $\alpha_1$ -AT polymerization, we have used the computation assisted design strategy SCADS<sup>50,51</sup> as described below.



**Structure template**—The WMDF-bound antithrombin structure (1JVQ)<sup>35</sup> was used as the structural template to design peptide(s) to block  $\alpha_1$ -AT polymerization. The new peptide was designed as a tetrapeptide, located at P7-P4 position. For these sequence calculations, the coordinates of the backbone atoms were constrained to those of the WMDF peptide.

**Sequence design**—SCADS (statistical, computationally-assisted design strategy) is used for identifying amino acid probabilities from a given backbone structure. The method takes as input (a) a target structure, (b) the energy functions that quantify sequence-structure compatibility, and (c) a set of energetic or other constraints on the sequences. In the calculations, a backbone dependent rotamer library<sup>59</sup> was used, with 81 rotamers for each amino acid residue in the calculations. For calculating the side chain - backbone and side chain - side chain interaction energies, the AMBER potential<sup>60</sup> with a modified hydrogen bonding term<sup>61</sup> was used to quantify van der Waals, electrostatic, and hydrogen bonding energies. All such energies were measured with respect to a “reference energy” that depends upon amino acid identity and crudely approximates intramolecular energetic interactions in the unstructured and unbound state.<sup>38</sup> The output is the site-specific probabilities of the rotamers of each amino acid, which yield the site-specific amino acid probabilities that guide the sequence selection. In this method, the conformational energy has a conjugate inverse temperature  $T_c$ ; as reported previously the probabilities used for design purposes here were determined at  $T_c = 0.5$  mol/kcal.<sup>37</sup>

## Materials

**Expression and Purification of the C232S/S359C  $\alpha_1$ -Antitrypsin Variant**—The protocols used to prepare the  $\alpha_1$ -antitrypsin variant used in the current study have been described in detail previously.<sup>30</sup>

**Preparation of P1'-TMR-Labeled  $\alpha_1$ -Antitrypsin**—C232S/S359C- $\alpha_1$ -antitrypsin was reacted with excess tetramethylrhodamine (TMR) dye and excess of buffer C (tris-(2-carboxyethyl)phosphine hydrochloride (Molecular Probes) in 5 mL of 50 mM Tris/50 mM KCL buffer, pH 8.3). The reaction was allowed to proceed overnight in dark at 4 °C and was quenched by excess  $\beta$ -mercaptoethanol. Excess dye was removed following the protocol reported earlier.<sup>30</sup> The extent of labeling of AT at the P1' position was determined using the TMR extinction coefficient of  $52000 \text{ M}^{-1}\text{cm}^{-1}$  at its isosbestic point and was found to be 1.04 TMR/protein. Protein concentration was determined by the bicinchoninic acid (BCA, Pierce, Rockford, IL) assay.

**Peptide Synthesis**—The peptides (WMDF, VIKF, VEIF, DIIF, VIID and FLKK) used in the current study were synthesized by standard solid phase Fmoc based peptide synthesis protocols on an automated peptide synthesizer (Protein Technologies Inc.). The peptides were then cleaved from the resin and subsequently purified by reverse phase HPLC. Each of the purified peptides had the appropriate mass as determined by electrospray mass ionization spectrometry.

## Depolymerizing Experiments by PAGE Analysis

TMR-labeled  $\alpha_1$ -AT (7.0  $\mu\text{M}$ ) in 50 mM Tris/50 mM KCL buffer (pH 8.3) was initially incubated at 45 °C for 24 hours to ensure complete polymerization. It was then mixed with 200-fold molar excess peptide (VIKF) and aliquots were removed at various time points, and brought to room temperature by dilution with 5 volumes of the same buffer. Samples were analyzed by non-denaturing polyacrylamide gradient gels (4-15%, BioRad, Hercules, CA) as previously described<sup>30</sup>. Protein was visualized by silver staining. Densitometric analysis was performed using NIH Image software, version 1.61.

## Blocking and Depolymerizing Experiments by FCS

For the blocking experiments, two protein samples, one containing 7  $\mu\text{M}$  TMR-labeled  $\alpha_1$ -AT and another containing 7  $\mu\text{M}$  of TMR-labeled  $\alpha_1$ -AT plus 1.4 mM WMDF (the concentration of WMDF was determined by tryptophan absorbance at 280 nm using  $\epsilon_{280} = 5600 \text{ M}^{-1}\text{cm}^{-1}$ ), were incubated at either 39 or 52  $^\circ\text{C}$ . At predetermined time intervals aliquots were removed and quickly diluted with buffer solution (Tris/KCl, pH = 8.3) at room temperature (23  $^\circ\text{C}$ ) to give a final concentration of 1 nM in  $\alpha_1$ -AT. This procedure halts further polymerization or depolymerization.<sup>30</sup> Diluted samples were used immediately for FCS measurements. The total observation time for each FCS measurement is 100 seconds with an integration time of 100  $\mu\text{s}$  for each point. Typically at least 30 to 35 such measurements were taken (for data presented in Figure 4) for each diluted sample. A similar protocol was followed for the depolymerization experiments, in which 7  $\mu\text{M}$  TMR-labeled  $\alpha_1$ -AT was first incubated at 45  $^\circ\text{C}$  for about 36 hours to ensure the formation of significant amount of  $\alpha_1$ -AT polymers.<sup>30</sup> In the following step, the temperature was decreased to 39  $^\circ\text{C}$  and the tetrapeptide of interest was added in 200-fold molar excess from stock solutions made up in 50 mM Tris buffer (pH 8.3). Concentrations of VIKF, VEIF and FLKK were determined by phenylalanine absorbance, using  $\epsilon_{257} = 197 \text{ M}^{-1}\text{cm}^{-1}$ . Aliquots were removed each day and quickly diluted with buffer solution at room temperature to give a final  $\alpha_1$ -AT concentration of 1 nM. At least 50 independent FCS traces (Figures 5 and 6) were collected for each diluted sample.

## FCS Measurements

FCS is based on the measurement of temporal intensity fluctuations caused by one or several fluorescent molecules diffusing in and out of a well-defined excitation volume element,<sup>45-57</sup> and the characteristic autocorrelation function  $G(\tau)$  can be obtained by correlating photon bursts according to the following equation:

$$G(\tau) = \frac{\langle \delta F(t) \delta F(t+\tau) \rangle}{\langle F(t) \rangle^2} \quad (1)$$

where  $\delta F(t) = F(t) - \langle F(t) \rangle$  is the fluorescence intensity fluctuation at time  $t$ . The temporal decay of  $G(\tau)$  contains information about the characteristic timescales of the dynamic processes causing the fluorescence fluctuations, such as diffusion, binding reactions, triplet state blinking, and conformational changes, among others.<sup>47,48,55</sup>

The confocal fluorescence microscope used is similar to those described in other studies.<sup>55</sup> Briefly, the excitation source ( $\sim 270 \mu\text{W}$ ) at 514.5 nm was derived from the laser lines of an  $\text{Ar}^+$  laser (Spectra-Physics, Mt. View, CA), which was brought to a focus in the sample solution by a microscope objective (Nikon 100X, NA 1.3, oil-immersion). The emission was collected by the same objective and was separated from the excitation by a dichroic mirror. The confocal volume was defined by a 50  $\mu\text{m}$  pinhole. A single interference filter was used to allow only the fluorescence to pass through and reach the detector. Photon counting in real time was done by an avalanche photodiode detector (SPCM-AQR-16, Perkin-Elmer, Vaudreuil, Canada) and a data acquisition card (PCI-6602, National Instruments, Austin, TX). A computer program written in LABVIEW (National Instruments, Austin, TX) was used to control the data collection as well as the subsequent autocorrelation analysis. Prior to every experiment, the confocal microscope system was calibrated by FCS measurements of the characteristic diffusion time of R6G (Molecular Probes).

For a prolate ellipsoidal Gaussian observation volume the autocorrelation function  $G(\tau)$  arising from diffusion can be described by the following equation:<sup>55</sup>

$$G(\tau) = \frac{1}{N} \sum_{i=1}^n \left( \frac{f_i}{1 + \frac{\tau}{\tau_D}} \right) \left( \frac{1}{1 + \frac{\tau}{\omega^2 \tau_D}} \right)^{1/2} \quad (2)$$

where  $n$  represents the number of fluorescent species in solution,  $\tau$  is the lag time,  $\tau_D^i$  is the characteristic diffusion time of species  $i$  during which it resides in the observation volume,  $\omega$  signifies the axial ( $z_0$ ) to lateral ( $r_0$ ) dimension ratio of the volume element,  $N$  denotes the mean number of fluorescent molecules in the time limit  $\tau \rightarrow 0$ , i.e.,  $G(\tau \rightarrow 0) = 1/N$ , and  $f_i$  signifies the fraction of species  $i$  in the solution. For a specific confocal microscopic setup, the diffusion time ( $\tau_D$ ) is related to the diffusion constant ( $D$ ) through the following equation:

$$\tau_D = \frac{r_0^2}{4D} \quad (3)$$

where  $r_0 = 0.3 \mu\text{m}$  for our setup. For a spherical diffusing species, the hydrodynamic radius ( $R_h$ ) is related to the diffusion constant via the following Stokes-Einstein relationship:<sup>49</sup>

$$D = k_B T / 6\pi\eta R_h \quad (4)$$

where  $k_B$  is the Boltzmann constant,  $T$  is the absolute temperature, and  $\eta$  is the viscosity of the solvent.

#### ACKNOWLEDGEMENTS

This work was supported by the National Institutes of Health grants AG-10599 (to B.S.C. and F.G.), GM-61267 (to J.G.S.), GM-065978 (to F.G.), and the National Science Foundation grant DMR05-20020 (to J.G.S. and F.G.).

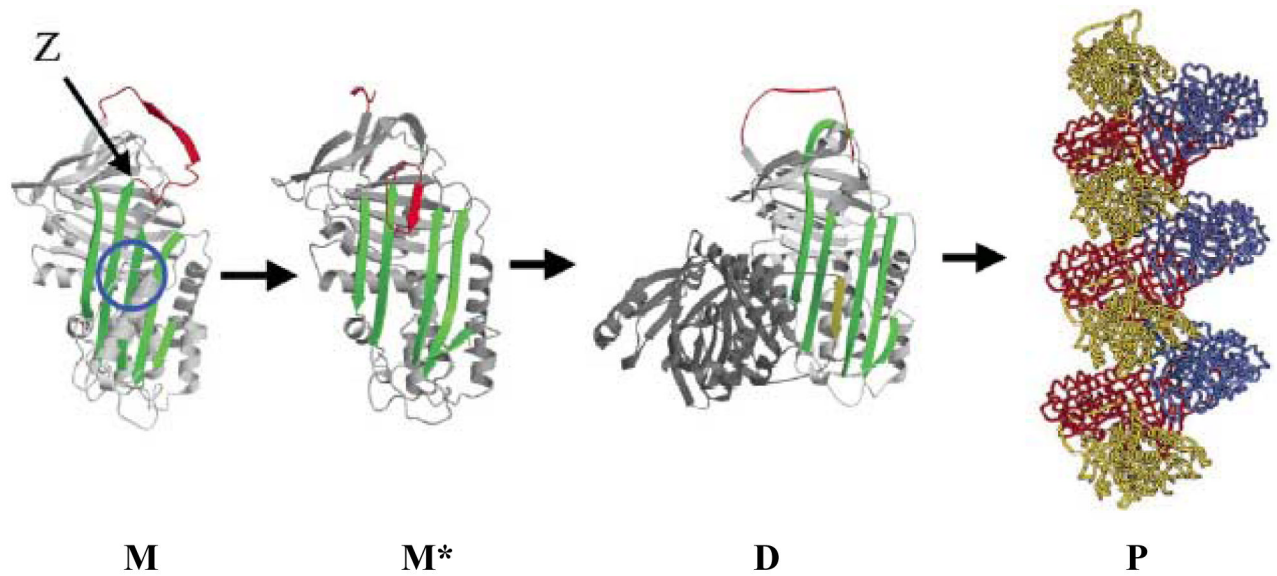
#### REFERENCES

1. Carrell RW, Huntington JA. How serpins change their fold for better and for worse. *Biochem. Soc. Symp* 2003;70:163–178. [PubMed: 14587291]
2. Gettins PG. Serpin structure, mechanism, and function. *Chem. Rev* 2002;102:4751–4804. [PubMed: 12475206]
3. Carrell, RW.; Boswell, DR. Proteinase inhibitors. Barrett, AJ.; Salvesan, G., editors. Elsevier; Amsterdam, The Netherlands: 1986. p. 403
4. Gettins P, Patston PA, Schapira M. The role of conformational change in serpin structure and function. *BioEssays* 1993;15:461–467. [PubMed: 8379949]
5. Mahadeva R, Dafforn TR, Carrell RW, Lomas D. 6-mer peptide anneals to a pathogenic serpin conformation and blocks polymerization. *J. Biol. Chem* 2002;277:6771–6774. [PubMed: 11773044]
6. Whisstock J, Skinner R, Lesk AM. An atlas of serpin conformations. *Trends Biochem. Sci* 1998;23:63–67. [PubMed: 9538691]
7. Devlin GL, Bottomley SP. A protein family under stress- serpin stability, folding and misfolding. *Front. Biosci* 2005;10:288–299. [PubMed: 15574369]
8. Loeberman H, Tokuoka R, Deisenhofer J, Huber R. Human  $\alpha_1$ -proteinase inhibitor: crystal structure analysis of two crystal modifications, molecular model and preliminary analysis of the implications for function. *J. Mol. Biol* 1984;177:531–556. [PubMed: 6332197]
9. Elliot PR, Stein PE, Bilton D, Carrell RW, Lomas DA. Structural explanation for the deficiency of S  $\alpha_1$ -antitrypsin. *Nat. Struct. Biol* 1996;3:676–681. [PubMed: 8756325]
10. Mottonen J, Strand A, Symersky J, Sweet RM, Danley DE, Geoghegan KF, Gerard RD, Goldsmith EJ. Structural basis of latency in plasminogen activator inhibitor-1. *Nature* 1992;355:270–273. [PubMed: 1731226]
11. Carrell RW, Stein PE, Wardell MR, Fermi G. Biological implications of a 3 Å structure of dimeric antithrombin. *Structure* 1994;2:257–270. [PubMed: 8087553]
12. Cabrita LD, Dai W, Bottomley SP. Different conformational changes within the F-helix occur during serpin folding, polymerisation and proteinase inhibition. *Biochemistry* 2004;43:9834–9839. [PubMed: 15274637]
13. Cabrita LD, Bottomley SP. How protein folds avoid becoming too stable? Biophysical studies into metastable proteins. *Eur. Biophys. J* 2004;33:83–88. [PubMed: 14504841]
14. Huntington JA, Read RH, Carrell RW. Structure of a serpin-protease complex shows inhibition by deformation. *Nature* 2000;407:923–926. [PubMed: 11057674]

15. Straikos E, Gettins PG. Formation of the covalent serpin-proteinase complex involves translocation of the proteinase by more than 70 Å and full insertion of the reactive center loop into β-sheet. *Proc. Natl. Acad. Sci. USA* 1999;96:4808–4813. [PubMed: 10220375]
16. Irving JA, Cabrita LD, Rossjohn J, Pike RN, Bottomley SP, Whisstock JC. The 1.5 Å crystal structure of a prokaryote serpin: controlling conformational change in a heated environment. *Structure* 2003;11:387–397. [PubMed: 12679017]
17. Mast AE, Enghild JJ, Salvesan G. Conformation of the reactive site loop of alpha1-proteinase inhibitor probed by limited proteolysis. *Biochemistry* 1992;31:2720–2728. [PubMed: 1547212]
18. Sivasothy P, Dafforn TR, Gettins PG, Lomas DA. Pathogenic alpha1-antitrypsin polymers are formed by reactive loop-beta-sheet A linkage. *J. Biol. Chem* 2000;275:33663–33668. [PubMed: 10924508]
19. Lomas DA, Belorgey D, Mallya M, Miranda E, Kinghorn KJ, Sharp LK, Philips RL, Page R, Robertson AS, Crowther DC. Molecular mousetraps and the serpinopathies. *Biochem. Soc. Trans* 2005;33:321–330. [PubMed: 15787598]
20. Huntington JA, Pannu NS, Hazes B, Read RJ, Lomas DA, Carrell RW. A 2.6 Å structure of a serpin polymer and implications for conformational disease. *J. Mol. Biol* 1999;293:449–455. [PubMed: 10543942]
21. Dunstone MA, Dai W, Whisstock JC, Rossjohn J, Pike RN, Feil SC, Le Bonniec BF, Parker MW, Bottomley SP. Cleaved antitrypsin polymers at atomic resolution. *Protein Sci* 2000;9:417–420. [PubMed: 10716194]
22. Sveger TN. Liver disease in alpha1-antitrypsin deficiency detected by screening of 200,000 infants. *Engl. J. Med* 1976;294:1316–1321.
23. Eriksson S, Carlson J, Velez RN. Risk of cirrhosis and primary liver cancer in alpha1-antitrypsin deficiency. *Engl. J. Med* 1986;314:736–739.
24. Eriksson S. Studies in alpha1-antitrypsin deficiency. *Acta Med. Scand. Suppl* 1965;432:1–85. [PubMed: 4160491]
25. Lomas DA, Carrell RW. Human genetics and disease: serpinopathies and the conformational dementias. *Nat. Rev. Genet* 2002;3:759–768. [PubMed: 12360234]
26. Carrell RW, Lomas DA. Conformational changes and disease – serpins, prions and Alzheimer's. *Curr. Opin. Struct. Biol* 1998;8:799–809. [PubMed: 9914261]
27. Lomas DA, Finch JT, Seyama K, Nukiwa T, Carrell RW. α<sub>1</sub>-Antitrypsin Siiyama (Ser53 → Phe). Further evidence for intracellular loop-sheet polymerization. *J. Biol. Chem* 1993;268:15333–15335. [PubMed: 8340361]
28. Dafforn TR, Mahadeva R, Elliott PR, Sivasothy P, Lomas DA. A kinetic mechanism for the polymerisation of α<sub>1</sub>-antitrypsin. *J. Biol. Chem* 1999;274:9548–9555. [PubMed: 10092640]
29. James EL, Bottomley SP. The mechanism of α<sub>1</sub>-antitrypsin polymerisation probed by fluorescence spectroscopy. *Arch. Biochem. Biophys* 1998;356:296–300. [PubMed: 9705220]
30. Purkayastha P, Klemke JW, Lavender S, Martinez RO, Cooperman BS, Gai F. α<sub>1</sub>-Antitrypsin polymerisation: A fluorescence correlation spectroscopic study. *Biochemistry* 2005;44:2642–2649. [PubMed: 15709777]
31. Chang WW-S, Wardell MR, Lomas DA, Carrell RW. Probing serpin reactive-loop conformations by proteolytic cleavage. *Biochem. J* 1996;314:647–653. [PubMed: 8670081]
32. Skinner R, Chang W-SW, Jin L, Pei X, Juntington JA, Abrahams JP, Carrell RW, Lomas DA. Implications for function and therapy of a 2.9 Å structure of binary-complexed antithrombin. *J. Mol. Biol* 1998;283:9–14. [PubMed: 9761669]
33. Chang Y-P, Mahadeva R, Chang WW-S, Shukla A, Dafforn T, Chu Y-H. Identification of a 4-mer peptide inhibitor that effectively blocks the polymerization of pathogenic Z α<sub>1</sub>-antitrypsin. *Am. J. Resp. Cell. Mol. Biol* 2006;35:540–548.
34. Elliott PR, Pei XY, Dafforn TR, Lomas DA. Topography of a 2.0 Å structure of α<sub>1</sub>-antitrypsin reveals target for rational drug design to prevent conformational disease. *Protein Sci* 2000;9:1274–1281. [PubMed: 10933492]
35. Zhou A, Stein PE, Huntington JA, Sivasothy P, Lomas DA, Carrell RW. How small peptides block and reverse serpin polymerization. *J. Mol. Biol* 2004;342:931–941. [PubMed: 15342247]
36. Zou J, Saven JG. Statistical theory of combinatorial libraries of proteins. Energetic discrimination of a target structure. *J. Mol. Biol* 2000;296:281–294. [PubMed: 10656832]

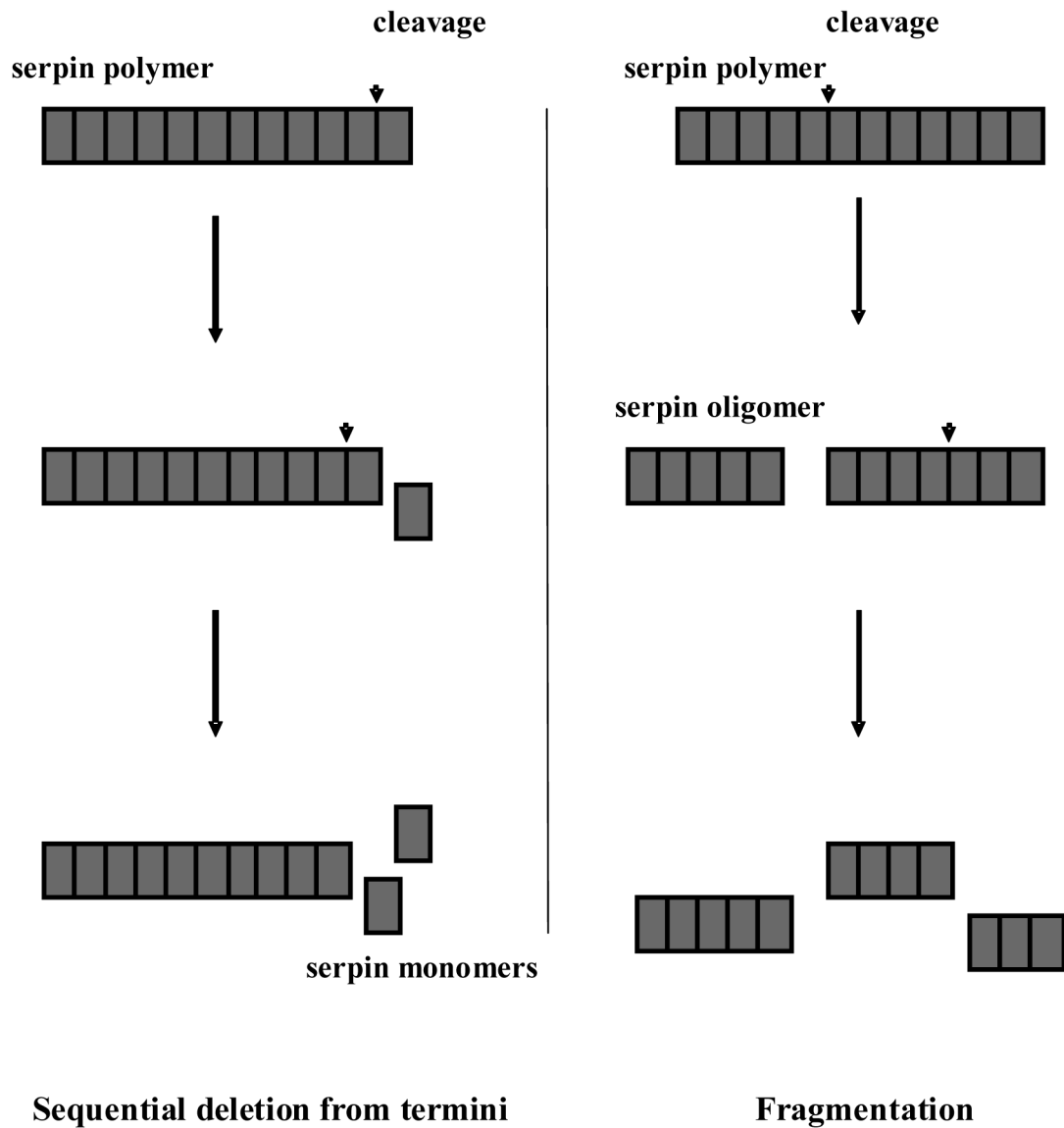
37. Kono H, Saven JG. Statistical theories for protein combinatorial libraries. Packing interactions, backbone flexibility, and the sequence variability of a main-chain structure. *J. Mol. Biol* 2001;306:607–628. [PubMed: 11178917]
38. Calhoun JR, Kono H, Lahr S, Wang W, Degrado WF, Saven JG. Computational design and characterization of a monomeric helical dinuclear metalloprotein. *J. Mol. Biol* 2003;334:1101–1115. [PubMed: 14643669]
39. Zhu Y, Fu X, Wang T, Tamura A, Takada S, Saven JG, Gai F. Guiding the search for a protein's maximum rate of folding. *Chem. Phys* 2004;307:99–109.
40. Bunagan MR, Yang X, Saven JG, Gai F. Ultrafast folding of a computationally designed Trp-cage mutant: Trp<sup>2</sup>-cage. *J. Phys. Chem. B* 2006;110:3759–3763. [PubMed: 16494434]
41. Slovic AM, Kono H, Lear JD, Saven JG, DeGrado WF. Computational design of water soluble analogues of the potassium channel KcsA. *Proc. Natl. Acad. Sci. USA* 2004;101:1828–1833. [PubMed: 14766985]
42. Cochran FV, Wu SP, Wang W, Nanda V, Saven JG, Therien MJ, DeGrado WF. Computational de novo design and characterization of a four-helix bundle protein that selectively binds a non-biological cofactor. *J. Am. Chem. Soc* 2005;127:1346–1347. [PubMed: 15686346]
43. Nanda V, Rosenblatt MM, Osyczka A, Kono H, Getahun Z, Dutton PL, Saven JG, DeGrado WF. De Novo Design of a Redox Active Minimal Rubredoxin Mimic. *J. Am. Chem. Soc* 2005;127:5804–5805. [PubMed: 15839675]
44. Swift J, Wehbi WA, Kelly BD, Stowell XF, Saven JG, Dmochowski IJ. Design of Functional Ferritin-like Proteins with Hydrophobic Cavities. *J. Am. Chem. Soc* 2006;128:6611–6619. [PubMed: 16704261]
45. Magde D, Elson EL, Webb WW. Thermodynamic fluctuations in a reacting system—measurement by fluorescence correlation spectroscopy. *Phys. Rev. Lett* 1972;29:705–711.
46. Magde D, Elson EL, Webb WW. Fluorescence correlation spectroscopy. II. An experimental realization. *Biopolymers* 1974;13:29–61. [PubMed: 4818131]
47. Davis LM, Shen G. Accounting for triplet and saturation effects in FCS measurements. *Curr. Pharm. Biotech* 2006;7:287–301.
48. Hess ST, Huang S, Heikal AA, Webb WW. Biological and chemical applications of fluorescence correlation spectroscopy: A review. *Biochemistry* 2002;41:697–705. [PubMed: 11790090]
49. Scwille P, Hausteiner E. Fluorescence correlation spectroscopy. An introduction to its concepts and applications. *Biophysics Textbook Online* 2001;Single Molecule Techniques:1–33.
50. Tjebberg LO, Pramanik A, Bjorling S, Thyberg P, Thyberg J, Nordstedt C, Berndt KD, Terenius L, Rigler R. Amyloid  $\beta$ -peptide polymerisation studied using fluorescence correlation spectroscopy. *Chem. Biol* 1999;6:53–62. [PubMed: 9889152]
51. Weidemann T, Wachsmuth M, Tewes M, Rippe K, Langowski J. Analysis of ligand binding by two-color fluorescence cross-correlation spectroscopy. *Single Mol* 2002;3:49–61.
52. Schwille P, Koriach J, Webb WW. Fluorescence correlation spectroscopy with single molecule sensitivity on cell and model membranes. *Cytometry* 1999;36:176–182. [PubMed: 10404965]
53. Kask P, Palo K, Ullmann D, Gall K. Fluorescence-intensity distribution analysis and its application in biomolecular detection technology. *Proc. Natl. Acad. Sci. USA* 1999;96:13756–13761. [PubMed: 10570145]
54. Pramanik A, Jureus A, Langel U, Bartfai T, Rigler R. Fluorescence correlation spectroscopy detects galanin receptor diversity on insulinoma cells. *Biochemistry* 2001;40:10839–10845. [PubMed: 11535060]
55. Eigen M, Rigler R. Sorting single molecules: application to diagnostics and evolutionary biotechnology. *Proc. Natl. Acad. Sci. USA* 1994;91:5740–5747. [PubMed: 7517036]
56. Chattopadhyay K, Saffarian S, Elson EL, Frieden C. Measurement of microsecond dynamic motion in the intestinal fatty acid binding protein by using fluorescence correlation spectroscopy. *Proc. Natl. Acad. Sci. USA* 2002;99:14171–14176. [PubMed: 12381795]
57. Chattopadhyay K, Saffarian S, Elson EL, Frieden C. The kinetics of conformational fluctuations in an unfolded protein measured by fluorescence method. *Proc. Natl. Acad. Sci. USA* 2002;102:2385–2389. [PubMed: 15701687]

58. Parfrey H, Dafforn TR, Belorgey D, Lomas DA, Mahadeva R. Inhibiting polymerization. New therapeutic strategies for  $Z\alpha_1$ -antitrypsin-related emphysema. *Am. J. Respir. Cell Mol. Biol* 2004;31:133–139. [PubMed: 15016619]
59. Dunbrack RL, Cohen FE. Bayesian statistical analysis of protein side-chain rotamer preferences. *Protein Sci* 1997;6:1661–1681. [PubMed: 9260279]
60. Weiner SJ, Kollman PA, Nguyen DT, Case DA. An all atom force field for simulations of proteins and nucleic acids. *J. Comp. Chem* 1986;7:230–252.
61. Kono H, Doi J. A new method for side-chain conformation prediction using a hopfield network and reproduced rotamers. *J. Comp. Chem* 1996;17:1667–1683.



**Figure 1.**

Structure of  $\alpha_1$ -antitrypsin (M) with the  $\beta$ -sheet A in green and the mobile RCL in red. Polymer formation results from Z-mutation (Glu342→Lys, as indicated by arrow) or aberrant opening of shutter domain to form an unstable intermediate, M\*. The  $\beta$ -sheet accepts a loop from another molecule to form a dimer D that finally extends to polymers P. Each  $\alpha_1$ -AT molecule in the polymer is shown in a different color (Reproduced with permission from: D.A. Lomas, D. Belorgey, M. Mallya, E. Miranda, K.J. Kinghorn, L.K. Sharp, R.L. Phillips, R. Page, A.S. Robertson and D.C. Crowther, 2005, *Biochemical Society Transactions*, **33**, 321-330. © the Biochemical Society).

**Figure 2.**

A schematic representation of the two possible modes of serpin depolymerization. The sequential deletion mode only involves cleavage of monomeric units from the end of a serpin polymer, whereas the fragmentation mode is characterized by breaking up a longer polymer into two shorter pieces.



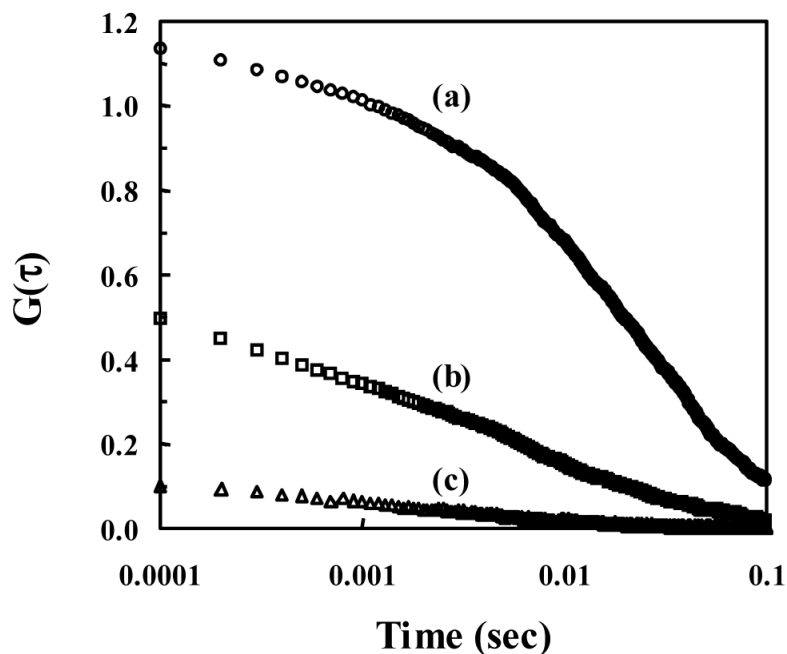


**Figure 3.**

Representative FCS traces corresponding to different reaction times of the depolymerization of  $\alpha_1$ -AT by WMDF obtained at 39 °C: (a) Day 1, (b) Day 14, and (c) Day 24. These data were modeled by Eq. (2) with two components. The fast component has a diffusion time of  $\sim 200$   $\mu$ s and was attributed to residual amount of free dye molecules present in the sample, whereas the slow component was assigned to TMR-labeled  $\alpha_1$ -AT species (monomer/oligomer/polymer) diffusing in and out of the confocal volume. The corresponding diffusion times of the slow component are: (a)  $\tau_D = 30$  ms, (b)  $\tau_D = 10$  ms, and (c)  $\tau_D = 2.5$  ms. The concomitant decrease in both values of  $\tau_D$  and  $G(0)$  as a function of reaction time indicates depolymerization. Error in the reported diffusion times is estimated to be  $\sim \pm 15\%$ .

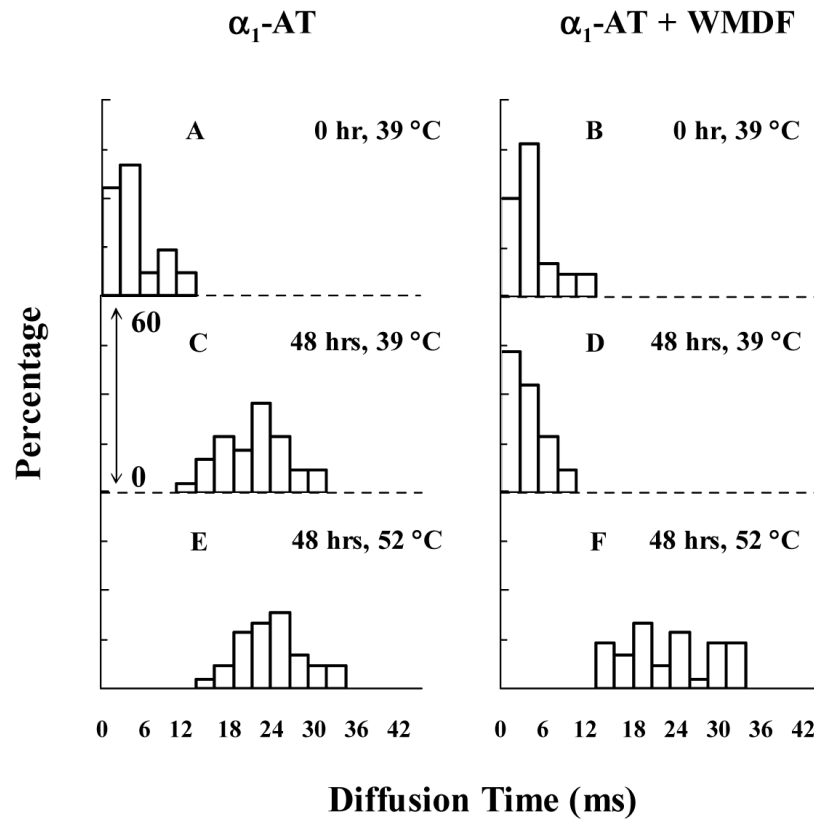


**Figure 4.** Distribution of diffusion times of  $\alpha_1$ -AT samples with and without the blocking peptide (WMDF). The incubation temperature was 39 °C for panels A-D and 52 °C for panels E and F. Width of the histogram corresponds to  $\Delta\tau_D = 3$  ms. Y-axis range for each panel is from 0 to 60 %.

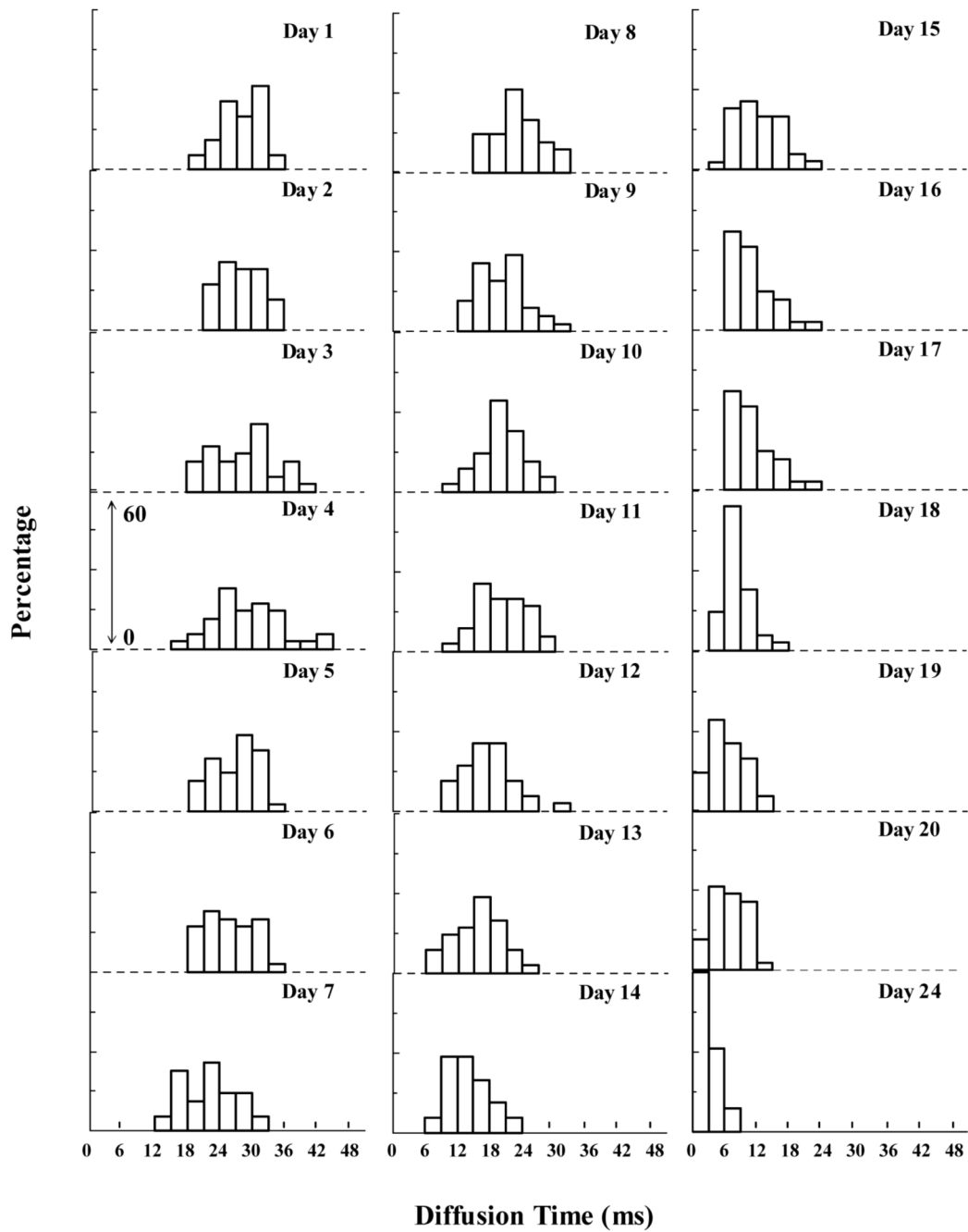


**Figure 5.** Distribution of diffusion times for  $\alpha_1$ -AT with WMDF (at 39 °C) as a function of the number of days incubated. Width of the histogram corresponds to  $\Delta\tau_D = 3$  ms. Y-axis range for each panel is from 0 to 60 %.

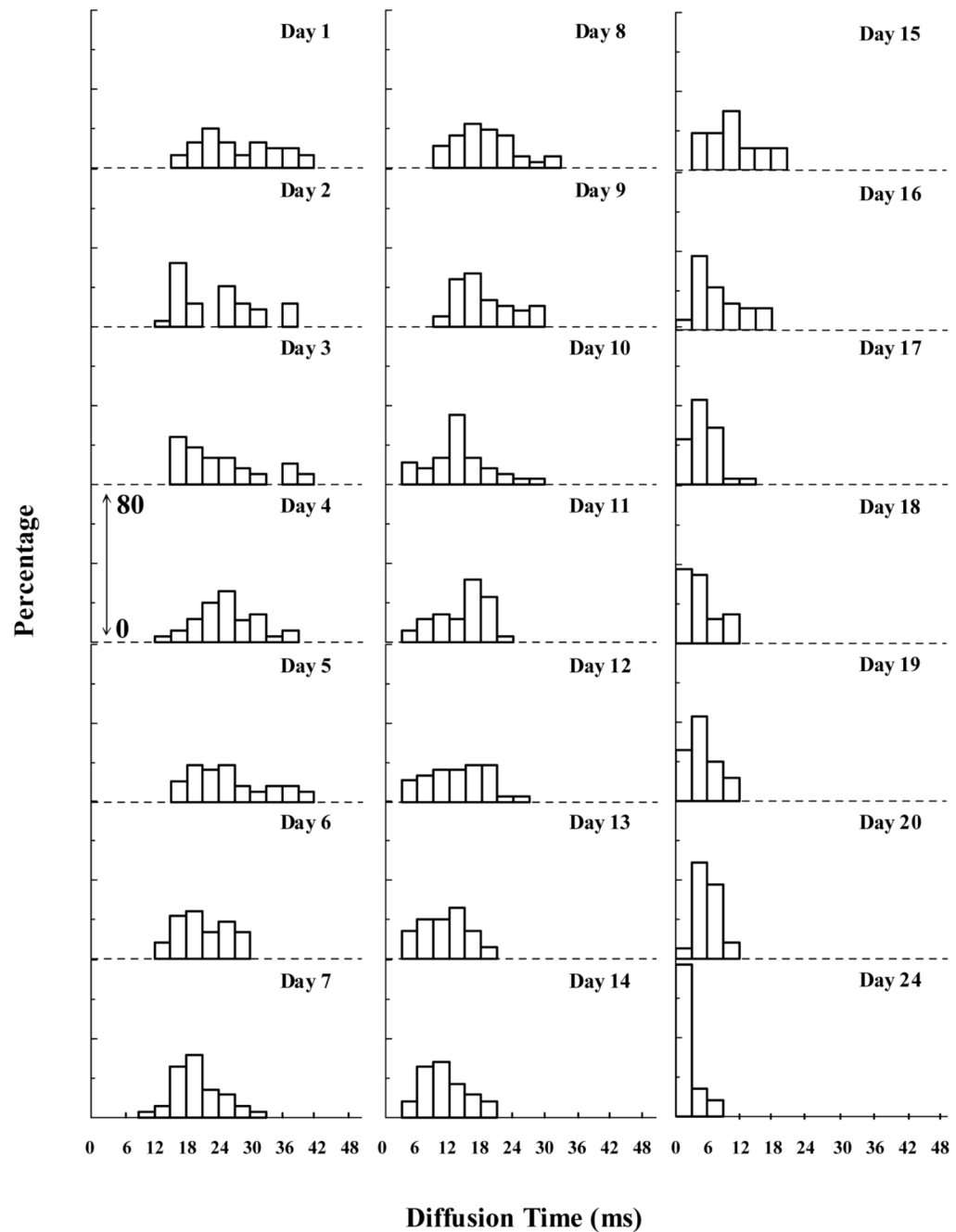


**Figure 6.** Distribution of diffusion times for  $\alpha_1$ -AT with VIKF (at 39 °C) as a function of the number of days incubated. The peptide concentration was kept at 200-fold molar excess over  $\alpha_1$ -AT. Width of the histogram corresponds to  $\Delta\tau_D = 3$  ms. Y-axis range for each panel is from 0 to 80 %.

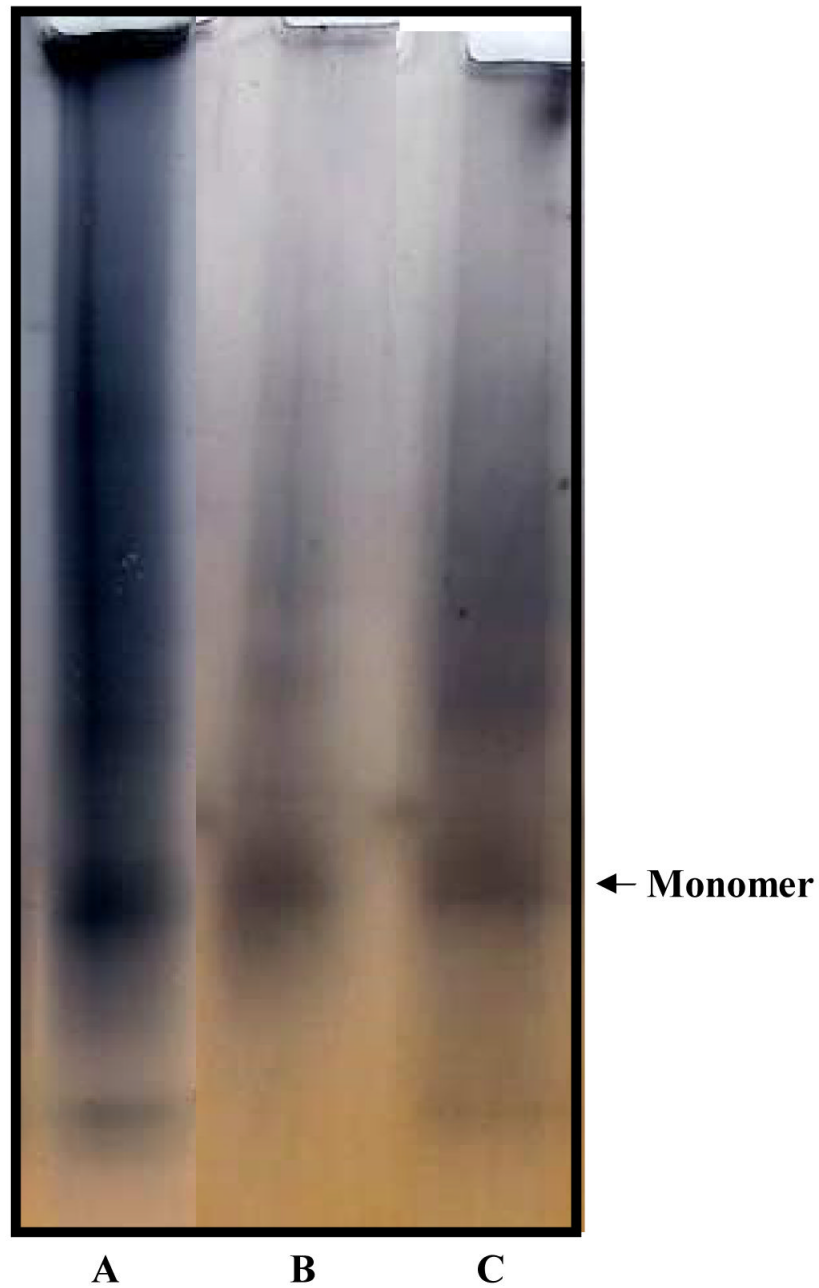


**Figure 7.** Nondenaturing PAGE analysis of the reversal of TMR-P1'-AT polymerization with VIKF. (A) TMR-labeled  $\alpha_1$ -AT polymers, (B) TMR-labeled  $\alpha_1$ -AT polymers + VIKF, incubated at 39 °C for 21 days, (C) Unheated TMR-labeled  $\alpha_1$ -AT. The position of the monomer band is shown.

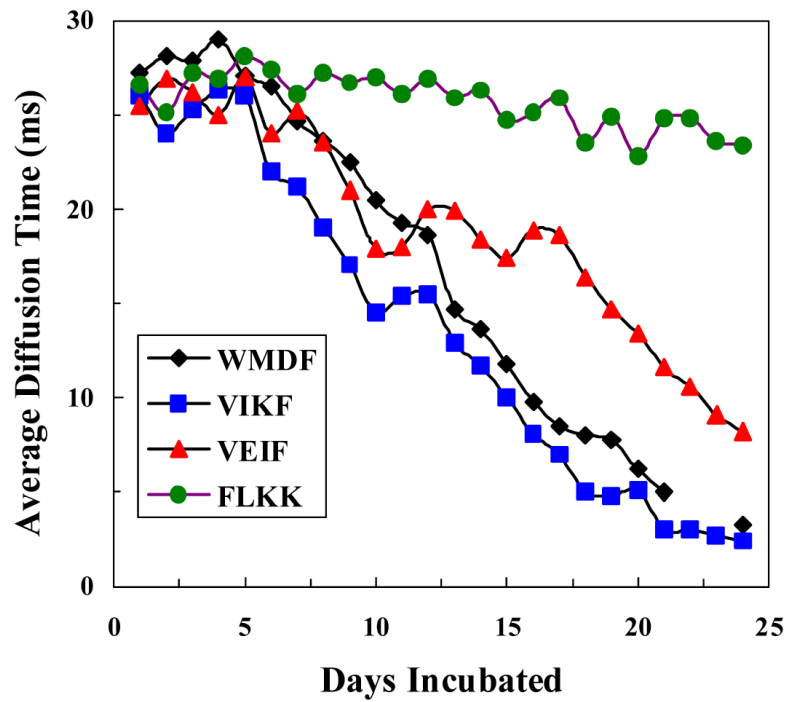


**Figure 8.** Average diffusion times vs. the number of days incubated for the depolymerizing peptides WMDF (black), VIKF (blue) and VEIF (red). In each case the diffusion times correspond to an average of at least 50 individual measurements. For comparison, the average diffusion time profile obtained for the control peptide FLKK (green) is also included.

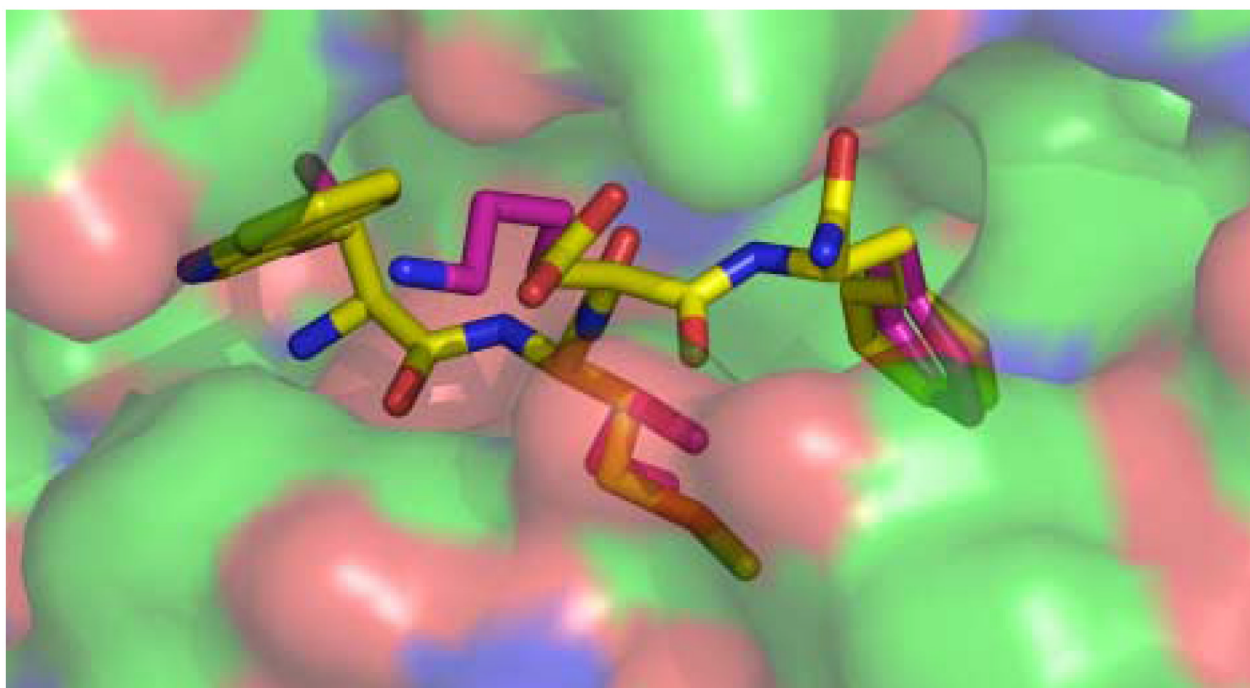


**Figure 9.** Peptides bound in the  $\beta$ -sheet A pocket of the serpin, antithrombin.<sup>32</sup> WMDF (yellow) bound to antithrombin, as it appears in the crystal structure of the complex (pdb code: 1JVQ).<sup>35</sup> Modeled structure of the designed peptide VIKF (magenta) containing the most probable rotamer states.